Polymer 67 (2015) A1–A13

Contents lists available at ScienceDirect

Polymer

journal homepage: www.elsevier.com/locate/polymer

Feature article

How does a polymer chain pass through a cylindrical pore under an elongational flow field?

Lianwei Li [a, *], Qianjin Chen [b], Fan Jin [c], Chi Wu [a, b, **]

[a] Hefei National Laboratory for Physical Sciences at the Microscale, Department of Chemical Physics, University of Science and Technology of China, Hefei, 230026, China
[b] Department of Chemistry, The Chinese University of Hong Kong, Shatin N. T., Hong Kong
[c] Hefei National Laboratory for Physical Sciences at the Microscale, Department of Polymer Science and Engineering, University of Science and Technology of China, Hefei, 230026, China

ARTICLE INFO

Article history:
Received 9 January 2015
Received in revised form
13 April 2015
Accepted 21 April 2015
Available online 29 April 2015

Keywords:
Translocation
Nanopore
Topology

ABSTRACT

How a polymer chain translocates through a cylindrical pore with its pore size smaller than the chain size (ultrafiltration behavior) is a fundamental question in polymer physics. Answering this question can provide broader implications and lead to potential applications for many applicable processes, such as gene transfection, protein transportation, and separation of a mixture of polymer chains. In the process of an electroneutral polymer chain passing through a nanopore, generally, an external flow with a sufficient high shear stress is needed to apply at the entrance of pore to induce a conformation change from a coil-like to a rod-like shape which is referred to as the "coil-to-stretch" transition, to squeeze into the pore. Up to last decade, many theoretical models have been built and carried out to predict how polymer chains pass through a nanopore. By contrast, rather limited experimental investigations have been performed to validate these theoretical predications, which is mainly because this kind of experimental study demands polymer chains with explicit topologies and nanopores with well-defined structures. Namely, 1) the polymer samples with narrow molecular-weight distributions, well-defined chain configurations, as well as hydrodynamic sizes larger than the pore radii; and 2) membranes with well-defined pore structure and isolated pore channels to prevent possible interaction between neighboring shearing flows.

In recent years, the development of polymer synthetic technology and the improvement of membrane manufacturing technology have stimulated a mass of research work on understanding the ultrafiltration behavior of polymer chains under an elongational flow field. In this feature article, the authors would like to mainly focus on the ultrafiltration behavior of flexible polymer chains with various topologies in dilute solution. More specifically, we will elucidate how the structural parameters of a polymer chain are related to the critical volumetric flow rate and the shape of polymer retention curve. Further application of this ultrafiltration method to the separation of polymer chain mixture and the rapid transformation among various polymer chain aggregated structures will be discussed. It is hoped that this perspective can provide a better view in understanding the translocation behavior of (bio)macromolecules in various practical processes and offer some guidance for the design and reality of commercially available ultrafiltration separation apparatus in the future.

1. Introduction

How a polymer chain translocates through a cylindrical pore with its pore size smaller than the chain size (ultrafiltration behavior) is a fundamental question in polymer physics [1–8]. Answering this question can provide broader implications and lead to potential applications for many applicable processes, such as gene transfection [9,10], protein transportation [11], and separation

* Corresponding author.
** Corresponding author. Hefei National Laboratory for Physical Sciences at the Microscale, Department of Chemical Physics, University of Science and Technology of China, Hefei, 230026, China.
E-mail addresses: llw@mail.ustc.edu.cn (L. Li), chiwu@cuhk.edu.hk (C. Wu).

http://dx.doi.org/10.1016/j.polymer.2015.04.063
0032-3861/

of polymer chain mixture by porous media [12–14], to name but a few. A simple view of the passage of polymers through porous media is purely geometrical, namely, in the dilute regime; the parameter that controls the passage of the chains is the ratio (λ) of the hydrodynamic radius (R_h) of a polymer chain to the pore radius (R_p): for $\lambda > 1$, the chains are excluded. The polymer translocation is generally viewed as an effective one-dimensionally activated process that involves overcoming the entropic loss, which is due to the decrease in the number of available chain conformations of the translocating molecules in comparison with the free chains.

The study on the ultrafiltration behavior of flexible polymer chains has received much attention in the past five decades [1–8,10,15–39]. Since 1965, Peterlin [8], Casassa [2], de Gennes [3,7], Pincus [4], and Daoudi and Brochard [5] have successively studied how a flexible linear chain passes through a cylindrical pore under a specific flow field. In particular, in 1966, Peterlin [8] first pointed out that there exists a critical strain rate for a linear chain under a flow velocity gradient, and the corresponding volumetric flow rate is called the critical volumetric flow rate ($q_{c,linear}$), at which a linear chain could go through a conformational change from a random coil to a stretched one to crawl through a nanopore with its size much smaller than the unperturbed size of the chain; later, de Gennes [3] and Pincus [4] systematically calculated this critical volumetric flow rate and found such a "coil-to-stretch" transition is first-order under an elongational shear flow and "second-order" under a vorticity shear flow; moreover, the calculated $q_{c,linear}$ should be independent of both the chain length and the pore diameter. Subsequent research was further extended to the estimation of critical volumetric flow rates of polymer chains with branched topologies [1,2,6,16,18,29].

However, theoretical research progress is far ahead of related experimental research due to the difficulty in the preparation of well-defined model samples and ultrafiltration membranes, and many important queries and theoretical predictions have not been experimentally clarified until recently. Namely, 1) the first-order "coil-to-stretch" transition of flexible linear polymer chains under elongational flow; 2) how the chain topology and parameter, as well as the pore structure affect the ultrafiltration behavior of polymer chains.

Owing to the development of polymer synthetic technology and the improvement of membrane manufacturing technology, a mass of research work have been devoted to understand the ultrafiltration behavior of polymer chains since the 1980s. The purpose of this feature article is mainly to provide a better view in understanding how the structural parameters of polymer chain and nanopore influence the translocation behavior of polymer chains through cylindrical channels. First, a brief introduction on the relevant theoretical background will be given, and the recently achieved experimental results on the translocation of polymer chains with different topologies through a cylindrical nanochannel will be discussed. Then, the advantages of utilizing ultrafiltration technique in the separation and characterization of polymer chains as well as polymer aggregated structures will be further described with some examples. Finally, we will summarize the whole article and give an outlook for the future research emphasis and challenge in this research field.

2. Classical theory: a review

2.1. Flory theory of a polymer chain in a good solvent

The translocation process of an electroneutral polymer chain through a nanopore under a flow velocity gradient is actually a dynamic process, where the polymer chain is forced to change its coiled conformation to stretched one under a fluid shear exerted by the movement of fluids over the surfaces of chain segments [40,41]. The whole process is associated with a decrease of the degree of freedom and an increase of the free energy (A) of polymer chain; however, it is not an easy task to clearly analyze how the size and free energy of an individual chain evolves in the whole dynamic process. Considering that it is much easier to capture the static properties of a given chain in its complete free or confined state, rather than in the translocation dynamic process, we'll first recall the Flory theory [42] to extract the static properties of a complete free or confined chain in solution. Based on Flory theory, the free energy of a real chain consists of two terms, the elastic energy ($A_e \sim R^2/R_0^2$) and the interaction energy ($A_i \sim b^3 N^2/R^3$), i.e. [42].

$$A/k_BT \approx \frac{R^2}{R_0^2} + \frac{b^3}{R^3}N^2 \tag{1}$$

where R and R_0 represent the sizes of a real and an idea chain, respectively; N is the degree of polymerization of a single chain; b is the monomer size; and k_B and T are the Boltzmann constant and the absolute temperature, respectively. The competition between A_e and A_i compromise an optimal size of R when $dA/dR = 0$, i.e.,

$$R \sim \left(R_0^2 N^2 b^3\right)^{1/5} \tag{2}$$

On the other hand, the unperturbed dimensions of linear, star and hyperbranched chains under θ condition can be expressed as [42–45].

$$R_0 \sim N^{1/2} b \quad \text{(linear)} \tag{3a}$$

$$R_0 \sim N^{1/2} b \frac{3f-2}{6f^2} \quad \text{(star)} \tag{3b}$$

$$R_0 \sim N_t^{1/4} N_b^{1/4} b \quad \text{(hyperbranched)} \tag{3c}$$

where f is the arm number of a star chain, and N_b and N_t are the degrees of polymerization of the subchain and the entirety of a hyperbranched chain, respectively. A combination of Eqs. (2) and (3a)–(3c) leads to the final expression of R, i.e.,

$$R \sim N^{3/5} b \quad \text{(linear)} \tag{4a}$$

$$R \sim N^{3/5} \frac{(3f-2)^{2/5}}{6^{2/5} f^{4/5}} b \quad \text{(star)} \tag{4b}$$

$$R \sim N_t^{1/2} N_b^{1/10} b \quad \text{(hyperbranched)} \tag{4c}$$

Generally, Eq. (4) can be used to roughly describe the initial states of various polymer chains before translocation through a nanopore. Similarly, Eq. (1) can also be extended to calculate the size of a polymer chain confined inside a cylindrical pore with a diameter of D. Assuming that the optimal length of the entire chain stretched along the flow direction inside a cylindrical pore is L, Eq. (1) can be rewritten as:

$$A/k_BT \approx \frac{L^2}{R_0^2} + \frac{b^3}{LD^2}N^2 \tag{5}$$

Therefore, optimal L can be found from $dA/dL = 0$, i.e.,

$$L \sim \left(\frac{R_0^2 b^3 N^2}{D^2}\right)^{1/3} \quad (6)$$

A combination of Eqs. (4) and (6) leads to

$$\frac{L}{D} \sim \left(\frac{R}{D}\right)^{5/3} \quad (7)$$

Eq. (7) reflects that the confined length is essentially determined by the chain size in good solvents and the pore diameter, irrelevant with the chain topology.

2.2. Critical volumetric flow rates of polymer chains with different topologies

A number of experiments have proved that Flory' approximation for the estimation of chain size is much more accurate than that for the estimation of free energy [42]. Therefore, the blob model developed by de Gennes [3,6,7] will be introduced here, for the estimation of free energy of a confined chain inside a cylindrical pore to derive the corresponding critical volumetric flow rate, at which a polymer chain could go through a conformational change from a randomly coiled conformation to a stretched one to squeeze through a nanopore.

As shown in Fig. 1A, the confined chain can be viewed as a string of blobs with the blob size $\xi = g_\xi^\alpha b$, where α is the Flory exponent and g_ξ is the monomer number in one blob. Under such confinement, the confinement energy (E_c) of each blob is on the order of thermal energy k_BT. The osmotic pressure (p) for each blob is $p \sim k_BT/\xi^3$, and the confinement force (f_c) is $f_c \sim p\xi^2 = k_BT/\xi$ [3,6,7]. On the other hand, the hydrodynamic force (f_h) from the fluid shear is proportional to the flow velocity (v) and the effective shear length (L_e), by $f_h = 3\pi\eta v L_e$, where $v = q/\xi^2$ and $L_e = \xi$; η and q are the solvent viscosity and microscopic volumetric flow rate, respectively. Therefore, for a confined chain with a confined length of l and a blob number of n_{blob} in a nanotube, the total confinement energy ($E_{c,t}$) can be expressed as:

$$E_{c,t} \sim k_BT \times n_{blob} = \frac{k_BTlD^2}{\xi^3} \quad (8)$$

On the other hand, the total hydrodynamic energy ($E_{h,t}$), i.e., the total work done by the shearing fluid can be expressed as:

$$E_{h,t} \sim \int_0^l dx f_h(x) \sim \frac{1}{2} l f_h(l) = \frac{3\pi\eta q\xi l^2}{2D^2} \quad (9)$$

Therefore, the overall energy barrier (E_{tot}) of a polymer chain which is needed to be overcome during the translocation process can be found, i.e. [3,6,7].

$$E_{tot} = E_{c,t} - E_{h,t} \sim \frac{k_BTlD^2}{\xi^3} - \frac{3\pi\eta q\xi l^2}{2D^2} \quad (10)$$

The corresponding optimal length (l^*) where E_{tot} has its maximum can be found when $dE_{tot}/dl = 0$:

$$l^* \sim \frac{2k_BTD^2}{3\pi\eta q\xi} \quad (11)$$

Essentially, only when the overall energy barrier is on the order of thermal energy k_BT, an individual chain can overcome the energy barrier by thermal motion. A combination of Eqs. (10) and (11) and $E_{tot} \sim k_BT$ leads to the final expression of the critical volumetric flow rate q_c as [7].

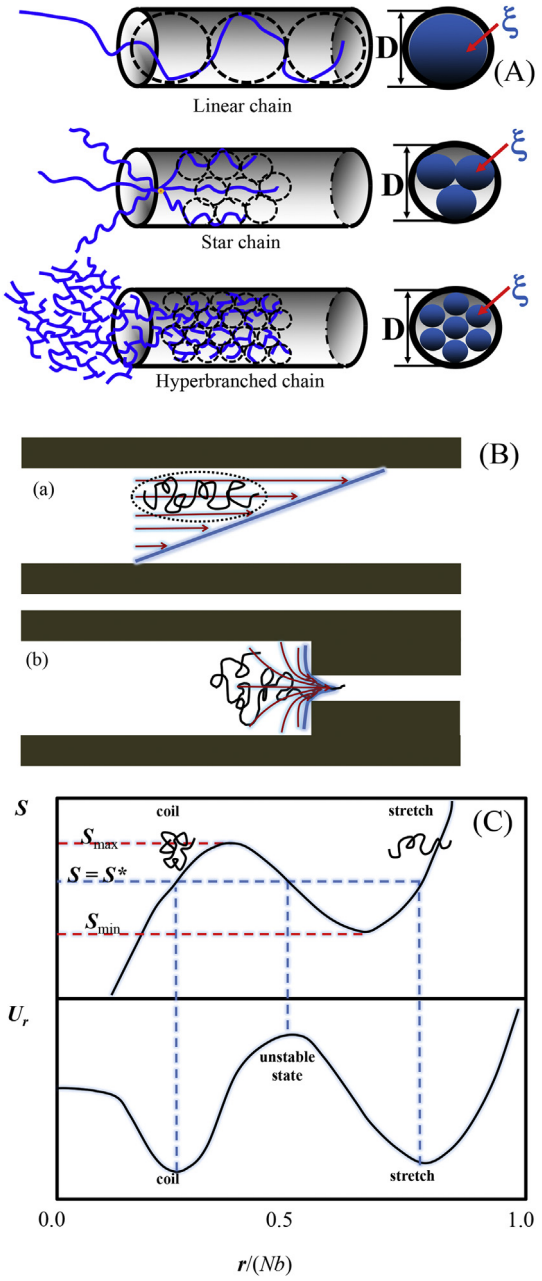

Fig. 1. (A) Schematic of confined blobs of polymer chains with different topologies inside a cylindrical pore; (B) Schematic illustration of a polymer chain sheared by typical (a) "transverse gradients" and (b) "longitudinal gradients" flow fields; and (C) Extension ratio ($\boldsymbol{r}/\langle Nb\rangle$) of a linear polymer chain dependence of shear rate (S) and chain potential (U_r) in a "longitudinal gradient".

$$q_c \sim \frac{k_BT}{3\pi\eta}\left(\frac{D}{\xi}\right)^4 \quad (12)$$

It should be emphasized that Eq. (12) was derived by de Gennes without any prior consideration of the chain topology. Putting the specific expression of blob size into Eq. (12), de Gennes derived the final expressions of q_c for linear, star and hyperbranched chains as [7].

$$q_{c,linear} \sim \frac{k_BT}{3\pi\eta} \quad \text{(linear)} \quad (13)$$

$$q_{c,star} \sim \frac{k_B T}{3\pi\eta}\left(\frac{f}{2}\right)^2 \quad (\text{star, symmetrical mode}) \tag{14a}$$

$$q_{c,star} \sim \frac{k_B T}{3\pi\eta} f\left(\frac{D}{Nb}\right)^{\frac{2}{3}} \quad (\text{star, asymmetrical mode}) \tag{14b}$$

$$q_{c,branch} \sim \frac{k_B T}{3\pi\eta}\left(\frac{N_t}{N_b}\right)^{\frac{1}{2}} \quad (\text{hyperbranched, strong confinement}) \tag{15a}$$

$$q_{c,branch} \sim \frac{k_B T}{3\pi\eta}\left(\frac{b}{D}\right)^{\frac{4}{3}} N_t^{\frac{2}{3}} N_b^{\frac{2}{15}} \quad (\text{hyperbranched, weak confinement}) \tag{15b}$$

The deduced results demonstrate that q_c is proportional to (D/ξ) with the fourth power. More specifically, 1) $q_{c,linear}$ is independent of both the chain length and the pore size; 2) under symmetrical model, $q_{c,star}$ is proportional to the second power of arm number, but under asymmetrical model, $q_{c,star}$ is not only proportional to the arm number, but also dependent on the arm length and the pore size; 3) $q_{c,branch}$ is scaled to both N_t and N_b, but different exponents are expected under strong and weak confinements. However, we will see that most of the experimental results deviate from these theoretical predictions.

2.3. The "coil-to-stretch" transition of a polymer chain under a flow field

After discussing the static properties of free and confined chains under a flow field, we will turn to discuss the corresponding dynamic properties of polymer chains in this section. Generally, the "coil-to-stretch" transition can occur only when a sufficiently strong shear rate is applied. More specifically, de Gennes [3] pointed out that the "coil-to-stretch" transition is a continuous second-order process in a "transverse gradients" flow field (Fig. 1B); while in a "longitudinal gradients" flow field (Fig. 1B), the transition is a discontinuous first-order process. Fig. 1C further shows how the effective potential (U_r) of polymer chain and the external shear rate (S) depend on the extension ratio during the first-order transition calculated by de Gennes, where $\boldsymbol{r}/(Nb) = 0.0$ and $\boldsymbol{r}/(Nb) = 1.0$, represent the ideal coiled and fully stretched states, respectively. It is shown that, in principle, it is possible for an individual chain to directly change its conformation from the coiled state to the stretched one through overcoming the energy barrier by thermal motion at $S = S^*$ when $S_{min} < S < S_{max}$, i.e., the first-order "coil-to-stretch" transition. It should be emphasized that the flow field at the entrance of a single pore is exactly a typical "longitudinal gradients" flow field, i.e., an elongational flow field. This means the first-order "coil-to-stretch" transition is expected in a real ultrafiltration experiment.

3. Unified theoretical description based on the balance of the confinement and hydrodynamic forces

3.1. Discrepancy between theoretical predictions and experimental results

Though the "coil-to-stretch" transition and the quantitative relation between the molecular parameter and the corresponding critical volumetric flow rate have been theoretically predicted in 1970s, the experimental observation was not obtained until recent years [18,21,24–26,28,32–34]. Especially, our group made much effort in this research field [16,18,21,25,26,28]. More specifically, we delicately designed and synthesized a series of polymer model samples, i.e., linear chains, star chains, and hyperbranched chains, and studied their ultrafiltration behavior. However, we found there existed big discrepancies between our experimental observation and de Gennes' theoretical prediction, e.g., 1) for linear chains, the observed $q_{c,linear}$ is indeed chain length-independent, but gradually decreases as the pore size increases, and $q_{c,linear}$ is 1–2 orders of magnitude smaller than the one predicted by de Gennes; 2) for star chains, the observed $q_{c,star}$ is arm length-independent, but proportional to the arm number ; 3) for randomly hyperbranched chains, $q_{c,branch}$ is scaled to both N_t and N_b, but the scaling exponents are different from the predicted ones; 4) the observed q_c is both chain-conformation and pore-size dependent. These discrepancies pushed us to rethink whether there is any improper assumption in de Gennes' deduction. In next section, a simple theoretical description developed by us will be introduced to illuminate the relation between the critical volumetric flow rate and the chain parameter by directly balancing the confinement and hydrodynamic forces on an individual confined "blob" [16]. Then, some important experimental results made by us and other groups will be presented and compared with the theoretical prediction.

3.2. Unified description of polymer chains passing through a cylindrical pore

As mentioned before, each polymer chain confined inside a small cylindrical pore can be viewed as a number of packed blobs, therefore, we only need to consider the balance of the confinement and hydrodynamic forces on an individual blob ($f_c = k_B T/\xi$ and $f_h = 3\pi\eta L_e v$, where v is the flow velocity and $v = q/D^2$, and L_e is the effective shear length of one blob along the flow direction and $L_e = \xi$), i.e., $f_c = f_h$. Using such an approach, we have established a unified description of normalized q_c without any prior consideration of the chain topology [16].

$$q_c \sim \frac{k_B T}{3\pi\eta}\left(\frac{D}{\xi}\right)^2 \tag{16}$$

It should be noted that the exponent in Eq. (16) is 2, while de Gennes' previously derived exponent is 4 (Eq. (12)). This is probably because the barrier energy (E_b) of one layer of the blobs was mistaken as ~ $k_B T$ in de Gennes' derivation, but $k_B T$ is actually the barrier energy for only one blob. In this case, the right expressions of q_c for polymer chains with different topologies should be:

$$q_{c,linear} \sim \frac{k_B T}{3\pi\eta} \quad (\text{linear}) \tag{17}$$

$$\frac{q_{c,star}}{q_{c,linear}} \sim \frac{f + |f - 2f_{in}|}{2} \quad (\text{star}) \tag{18}$$

$$\frac{q_{c,branch}}{q_{c,linear}} \sim \left(\frac{b}{D}\right)^{\frac{2(3-5\alpha)}{3(3\alpha-1)}} N_t^{\gamma} N_b^{\varphi} \quad (\text{hyperbranched}) \tag{19}$$

where γ and φ can be expressed as:

$$\gamma = \frac{\alpha}{3(3\alpha - 1)} \quad \text{and} \quad \phi = \frac{6\beta - \alpha}{3(3\alpha - 1)} \tag{20}$$

For the weak confinement, $\alpha = 1/2$ and $\beta = 1/10$ (branched structure inside a blob); while for the strong confinement, $\alpha = 3/5$ and $\beta = 0$ (linear structure inside a blob). Therefore, we have:

$$\frac{q_{c,branch}}{q_{c,linear}} \sim \left(\frac{b}{D}\right)^{\frac{2}{3}} N_{t,Kuhn}^{\frac{1}{3}} N_{b,Kuhn}^{\frac{1}{15}} \quad \text{(weak confinement)} \qquad (21a)$$

$$\frac{q_{c,branch}}{q_{c,linear}} \sim \left(\frac{N_{t,Kuhn}}{N_{b,Kuhn}}\right)^{\frac{1}{4}} \quad \text{(strong confinement)} \qquad (21b)$$

By equaling the right sides of Eqs. (21a) and (21b), we can get the critical pore size (D^*) between these two limits:

$$D^* \sim b N_{t,Kuhn}^{\frac{1}{8}} N_{b,Kuhn}^{\frac{19}{40}} \qquad (22)$$

Satisfyingly, this simple but unified description (Fig. 2) is supported by the experimental results [18,21,26,28] and the recent first principle calculation [22,23]. It is worth noting that for linear chain, only one blob can be found on the cross-section inside the cylindrical tube during translocation process. Thus, the exponent difference in Eqs. (12) and (16) is ignored because (D/ξ) is 1.0, which explains why, for a linear chain, the deduced results by us and de Gennes are the same.

4. Important experimental results

4.1. Experimental setup and characterization method

Before starting a real ultrafiltration experiment, a well-designed experimental setup needs to be established to accurately capture the retention concentration of the studied polymers. The most used experimental setups are shown in Fig. 3. Namely, the setup shown in Fig. 3A is composed of a peristaltic pump, an ultrafiltration membrane, a feed tank, and a transmembrane pressure sensor. During the experiments, the polymer solution is pumped from the feed tank to the ultrafiltration membrane at a constant rate, and the samples of retentate and permeate are taken for a given time interval and subsequently analyzed by ultraviolet-vis (UV) spectrometer or refractive index (RI) detector [24,33,34]. The advantage of this loop design is that the boundary layer effect at the high-pressure surface of the membrane can be reduced because the polymer chains are not allowed to accumulate at the membrane/solution interface. Considering that the experiment should be carried out in dilute solution, in which the polymer concentration should be typically ~ one tenth of the overlapping concentration of

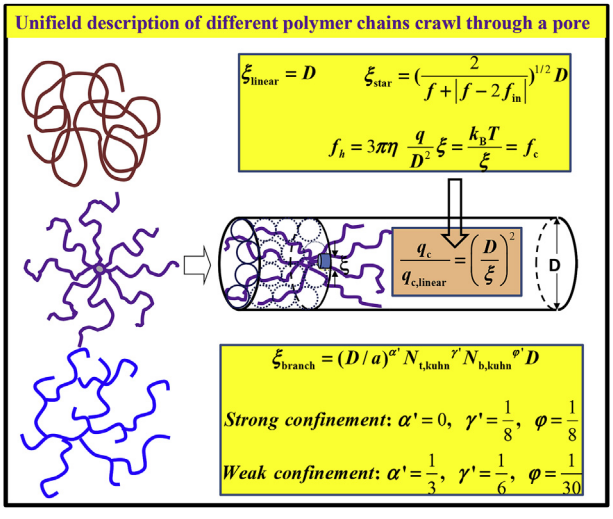

Fig. 2. Schematic of chains with different topologies confined inside a cylindrical pore and how the blob size (ξ) varies with chain topology.

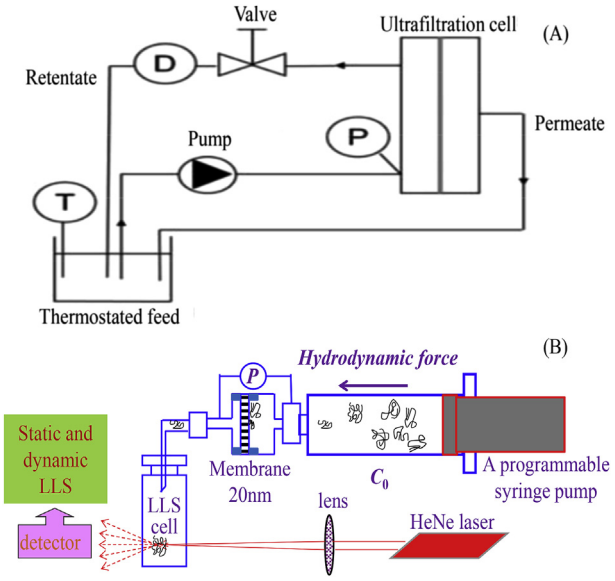

Fig. 3. Schematic illustrations of the ultrafiltration experimental setups.

the used polymer sample, the high molar mass samples ($M_w > 5 \times 10^6$ g/mol) with an extremely low overlapping concentration are generally limited in these experiments as the measurable concentration limit for UV and RI detectors is typically ~ 10^{-1} g/L. Fig. 3B shows the experimental setup developed by our group, and it is mainly composed of a programmable pump, a gas-tight syringe, an ultrafiltration membrane, a receiving cell and a laser light scattering (LLS) detector. In experiments, LLS detector is used as the scattered light intensity is proportional to the multiply of the molar mass and the mass concentration of a given polymer fraction, much more sensitive than that of UV and RI detectors; therefore, the measurable lower limit for high molar mass polymer can reach 10^{-2} ~ 10^{-3} g/L, which is much lower than the corresponding overlapping concentration. Moreover, some short chains with hydrodynamic radii much smaller than the nanopore radius are mixed with the studied long chains as internal standards to improve the accuracy of the measured concentration since short linear chains can pass through the nanopore without retention. Though dynamic loop structure is missed for this setup design, the tested injection volumetric flow rate in the study is low enough so that the polymer chains accumulated at the high-pressure surface have enough time to diffuse to weaken the boundary layer effect.

4.2. Translocation of a linear chain: effect of the chain length and conformation

The core concerns of the ultrafiltration behavior of polymer linear chains are related to: 1) whether the passage of linear chains through a small cylindrical pore is the first-order "coil-to-stretch" transition; 2) how the chain parameter affects the translocation process. Usually, most of the experimental results reported in literatures have been essentially performed in pressure driven ultrafiltration devices and basically consist of measuring the relative retention concentration [$(C_0 - C)/C_0$] of the studied polymers, where C_0 and C are the concentrations of polymer retentate and permeate [24,26,28,31,33,34]. However, most of studies [24,31,33,34] reported a smooth transition from total retention to forced penetration, except for us [26,28]. Namely, Beerlage et al. [31] investigated the retention behavior of linear polystyrenes in ethyl acetate. It was shown that the "coil-stretch" transition is not

precipitous, but gradual; and the critical volumetric flow rate is chain length and polymer concentration independent in dilute solution. Anderson et al. [32–34] explored the ultrafiltration behavior of linear polystyrenes through track-etched mica sheet in a mixed solvent of carbon tetrachloride and methanol. The result implied the critical flow rate is nearly independent on the chain length, pore size, and solvent quality, and the transition presents a smooth characteristic. In the semi dilute region, the critical volumetric flow rate was found to decrease significantly with polymer concentration. Neel et al. [35] studied the ultrafiltration behavior of polyethylene glycol (PEG) and dextran in water, where a relatively sharp transition was observed. Moreover, the result demonstrated that the critical volumetric flow rate is constant in dilute solution, nearly irrelevant with the chain length, but gradually decreases with concentration in the semi-dilute region. Recently, Duval et al. [24] measured the relative retention concentration of high molecular weight polyethylene oxide (PEO) in water by using track-etched polycarbonate porous media as membrane, where they transformed the measured $[(C_0 - C)/C_0]_{observed}$ into the true $[(C_0 - C)/C_0]_{true}$ by considering the boundary layer effect. The result indicated a smooth transition, as shown in Fig. 4A.

We started our "ultrafiltration-tour" from the study of narrowly distributed linear polystyrene in its good solvent toluene, in which we have not only observed the predicted "first-order" transition, but also clearly figured out how the chain length and conformation affect the critical volumetric flow rate [26,28]. In our initial attempt, two long linear polystyrenes with different hydrodynamic sizes ($\lambda = 0.9$ and 9.9) were comparatively studied, and the result clearly showed that the long polystyrene chains could be completely retained at low volumetric flow rate, but sharply passed through nanopores at the same volumetric flow rate ($q_{c,linear}$ ~4.4 × 10^{-14} mL/s) (Fig. 4B), different from the smooth transition observed by other groups. The observed $q_{c,linear}$ is indeed chain length independent, in good agreement with the observations of other groups. We attributed this sharp transition to the special double-layer structure of ultrafiltration membrane used in the study.

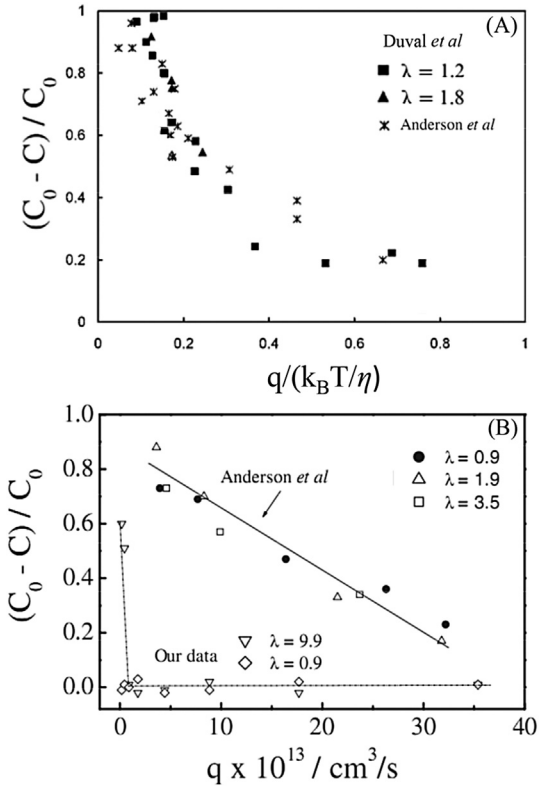

Fig. 4. Microscopic flow rate (q) dependence of relative retention concentration $[(C_0–C)/C_0]$, reported by (A) Duval et al. [24] and (B) Wu et al. [28], where λ represents the radius ratio of the chain and pore. For comparison, some results from Anderson et al. were plot [33,34]. Reproduced with permission [24,28].

As shown in Fig. 5, the scanning electron microscope (SEM) and pressure drop test of the ultrafiltration membrane used in our study demonstrated that each smaller 20 nm pore (layer B, length 1 μm) is solely under a 200 nm one (layer A, length 59 μm), which means during the translocation process, the chains are supposed to first pass through a 200 nm large pore (layer A), and then through the corresponding 20 nm small pore (layer B), i.e., from layer A to layer B. The merit of such double-layer structural membrane is the complete screening of the possible interaction between neighboring flow fields through the 20 nm nanopore entrances. This conjecture was further supported by following control experiment, namely, the translocation of polystyrene chains directly passing the 20 nm pores (layer B) without being screened by the 200 nm large pore (layer A) could result in a more smooth transition as well as a much higher critical volumetric flow rate, while in the reversal direction from 200 nm pore to 20 nm where the screening effect is present, the transition is much abrupt and sharp, as indicated in Fig. 4B. Such an experiment may explain why most of previously observed ultrafiltration transitions [24,31,34,35] were smooth, instead of sharp. In contrast, a continuously 3-dimentional network-like membrane is highly not recommended for the quantitative ultrafiltration-related study because of its poorly defined pore geometry. Generally, the interaction among flow fields will greatly dissipate fluid mechanical energy and reduce the effective shear force along the flow direction, leading to a larger apparent critical volumetric flow rate. The comparison of these experimental results reminds us that the structure of nanopore used in ultrafiltration experiment may play much more important role in regulating the polymer chain translocation behavior than we thought.

Though the existing experimental results [24,26,28,31,33,34] (Fig. 6A) and an abundant of computer simulation work [15,20,22,24] (Fig. 6B) support that the critical volumetric flow rate is independent on the chain length, in consistence with de Gennes's prediction, the origin of deviation of the measured q_c from the predicted $k_BT/(3\pi\eta)$ has been rarely discussed. Especially, the measured values of $q_{c,linear}$ were found to be ~10–200 times smaller than the predicted $k_BT/(3\pi\eta)$ in our experiments [3,7], and we attributed it to the improper assumption that each blob is a non-draining hard sphere. Instead, the actual hydrodynamic force f_h should be expressed as $f_h = 3\pi\eta(q/D^2)L_e$ [26], where L_e is the effective length along the flow direction. When $f_h = f_c$, q reaches its critical value, i.e.,

$$q_{c,linear} \sim \frac{k_B T}{3\pi\eta}\left(\frac{D^2}{\xi L_e}\right) \tag{23}$$

In de Gennes' derivation (Eq. (17)), each blob is considered as a non-draining sphere, and $L_e = \xi = D$; while for a fully draining blob

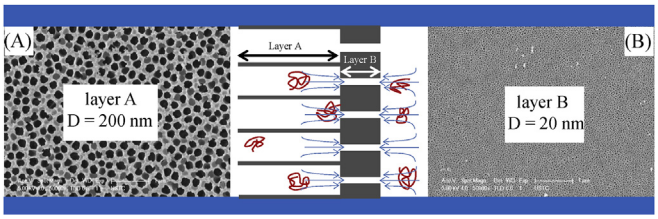

Fig. 5. Schematic of structure of the ultrafiltration membrane with a special double-layer structure, where the insets show the SEM images of layers A (200 nm) and B (20 nm).

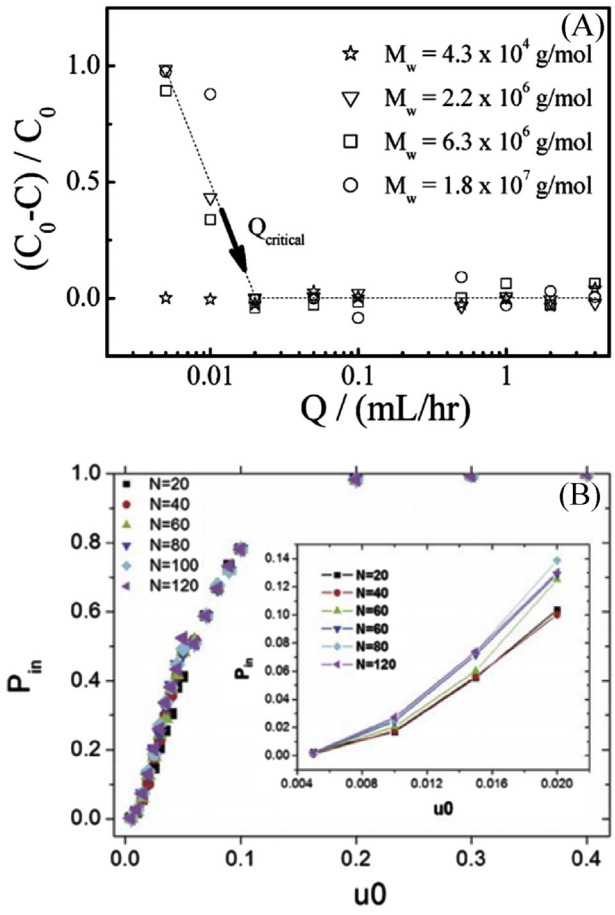

Fig. 6. (A) Macroscopic flow rate (Q) dependence of retention concentration [$(C-C_0)/C_0$] of polystyrene chains with different molar masses in cyclohexane at $T = 34.5$ °C (reported by Wu et al. [26]); and (B) Inlet fluid velocity (u0) dependence of transport probability (P_{in}) for different chain lengths under the condition of the head monomer of polymer chain anchored in the channel at the beginning of the transport process (reported by Yang et al. [15]). Reproduced with permission [15,26].

made of n segments and each with an average length of l, $L_e = ln$ and $n = M_b/M_0$, where M_b and M_0 are the molar masses of the blob and the segment, respectively. Considering that each blob has a size of D and using the scaling $D = kM_b^{\alpha}$, we have $L_e = nl = lM_b/M_0 = (l/M_0)(\xi/k)^{1/\alpha}$, where α is the Flory exponent and k is a constant for a given polymer solution. Eq. (23) can be rewritten as [26].

$$q_c \sim \frac{k_B T}{3\pi\eta}\frac{M_0}{l}\left(\frac{D}{\xi}\right)^2 k^{1/\alpha} D^{1-1/\alpha} \tag{24}$$

Quantitatively, taking the θ condition as a reference, the calculated values of $q_{c,linear}$ by Eq. (24) were found to satisfyingly agree with our experimental values. This simple scaling argument was further supported by the first principle calculation based on analytical Green's function/numerical inverse Laplace transform methods [22]. Satisfactory agreement between the calculated and observed critical volumetric flow rates (Fig. 7) revealed that the previous description by de Gennes of a linear chain confined in a tube as a series of hard spheres (blobs) significantly underestimates the hydrodynamic drag force. This finding has also provided some implication why linear RNA and protein chains with different lengths translocate through small nuclear pores without any collision [10]. Moreover, the experimental result showed that $q_{c,linear}$ experienced a decrease-increase-decrease (Fig. 7) process as temperature increased in cyclohexane, different with the conclusion of Anderson et al. [33] that $q_{c,linear}$ is independent of solvent

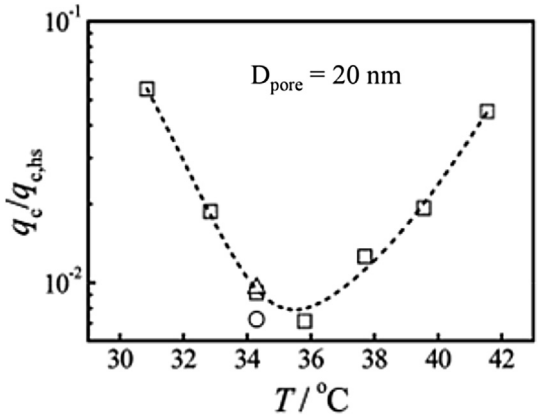

Fig. 7. Measured temperature dependence of the normalized critical volumetric flow rate ($q_c/q_{c,HS}$) for polystyrene in cyclohexane [26], where $q_{c,HS} = k_BT/(12\eta)$ and the circles and triangles represent the two calculated values, respectively. Reproduced with permission [22].

goodness. This conformation dependence should be attributed to the counterbalance between the entropic elasticity and some additional segment–segment attraction forces, which can also be quantitatively explained by Eq. (24) and the first principle calculation [22].

On the other hand, the modified theoretical description (Eq. (24)) predicts a scaling between q_c and D as $q_c \sim D^{1-1/\alpha}$, where α are 1/2 and 2/3 in θ and good solvents, respectively. Therefore, we further designed experiments to clarify this point. The results clearly indicated that $q_{c,linear}$ gradually decreases as the pore size increases from 20 to 100 nm at both $T = 34.3$ and 41.6 °C in cyclohexane [26], i.e., $q_{c,linear,20nm}/q_{c,linear,100nm} \simeq 8–10$, not far from the calculated value of 5 by Eq. (24), which directly verified the practicability of our unified description.

4.3. Translocation of a star chain: effect of the arm length and the arm number

In contrast to linear chains, the ultrafiltration of polymers with some complicated structure, such as star and branched configurations, through a nanopore is more intricate. In theory, a regular star polymer with f number of uniform arms joined at a central point might be the simplest case, but only few theoretical work have been reported in the last five decades [7,46–49]. Though the pioneering wok made by de Gennes and Brochard-Wyart showed that the critical volumetric flow rate ($q_{c,star}$) depends not only on the total arm number f, but also on the arm length (L); to the best of our knowledge, such predictions have only been experimentally tested by Anderson et al. [32] and subsequently by our group [21]. However, only some qualitative conclusion can be drawn by Anderson et al. [32] that the effect of branching of star chains on the critical volumetric flow rate is significant because only two star polystyrenes with both different arm lengths and different arm numbers were used in their study. Recently, using high vacuum anionic polymerization, we prepared two sets of well-defined star polystyrenes, namely, one set of star chains with different arm numbers but exactly an identical arm length, the other set with different arm lengths but an identical arm number, and further investigated their ultrafiltration behavior [21]. The results clearly showed that the critical volumetric flow rate of star polymer ($q_{c,star}$) is independent on the arm length (Fig. 8A), but strongly dependent on the arm number (Fig. 8B). Intuitively, the model of a star chain entering a nanopore can be divided into two different situations (Fig. 8C), namely, $1 \le f_{in} \le f/2$ and $f \ge f_{in} \ge f/2$. While both the

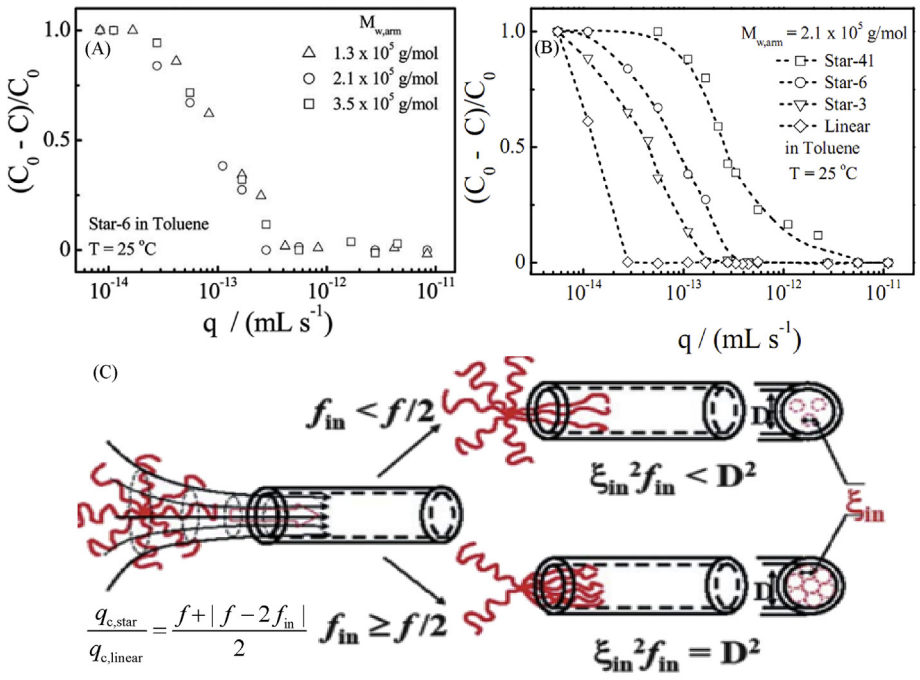

Fig. 8. (A) Flow rate (q) dependence of relative retention [$(C_0-C)/C_0$] of star chains with different arm lengths (L) but an identical arm number in toluene (reported by Wu et al. [21]); (B) Volumetric flow rate (q) dependence of relative retention [$(C_0-C)/C_0$] of star chains with different arm numbers (f) but an identical arm length in toluene (reported by Wu et al. [21]); and (C) Schematic of how a star chain enters a nanopore under two different situations, namely, $1 \leq f_{in} \leq f/2$ and $1 \geq f_{in} \geq f/2$. Reproduced with permission [21].

theoretical derivations by de Gennes (Eq. (14a)) and us (Eq. (18)) have shown that for a star polymer in a static solvent, the lowest energy barrier for entrying into a pore with a diameter smaller than the size of polymer chain occurs with a symmetric distribution of polymer arms inside the cylindrical tube. Therefore, it is reasonable to assume the experimentally measured $q_{c,star}$ to be the $q_{c,star}$ under symmetric model. Quantitatively, the measured $q_{c,star,50\%}$ is scaled to the arm length as $q_{c,star,50\%} \sim (f/2)^{0.95}$, where the exponent 0.95 is much smaller than that predicted by de Gennes (2.0) from Eq. (14a), but agrees well with the predicted value from our unified description (Eq. (18)).

4.4. Translocation of a hyperbranched chain: effect of the degrees of polymerization of the subchain and the whole chain

Compared with linear and star structures, randomly hyperbranched structure is much more complicated and there are only a few theoretical studies reported the ultrafiltration behavior of hyperbranched chains [6,7,29,51,52]. Until recently, using specially designed seesaw-type macromonomer, our group successfully prepared two sets of hyperbranched polystyrenes with different overall molar masses ($M_{w,t}$) but a uniform subchain length ($M_{w,b}$) or with different subchain lengths but a similar overall molar mass, and established the scaling laws between their sizes (R), intrinsic viscosities ([η]) and molar masses (M), namely, the intrinsic viscosities [η] of these hyperbranched chains are scaled to the degrees of polymerization of the branching subchain (N_b) and the whole chain (N_t) as: $[\eta] = K_\eta N_t^{0.39} N_b^{0.31}$ (Fig. 9A) [50]. These experimentally obtained scaling exponents agreed well with the theoretical values [45,53]. Such scaling relation has been recently supported by the general theory developed by An and his coworkers to describe the intrinsic viscosity of polymer chains with various topologies, where they separated the dissipation mechanism around a polymer into two key contributions-rotational friction and perturbation of the flow field by the polymer [54]. Armed

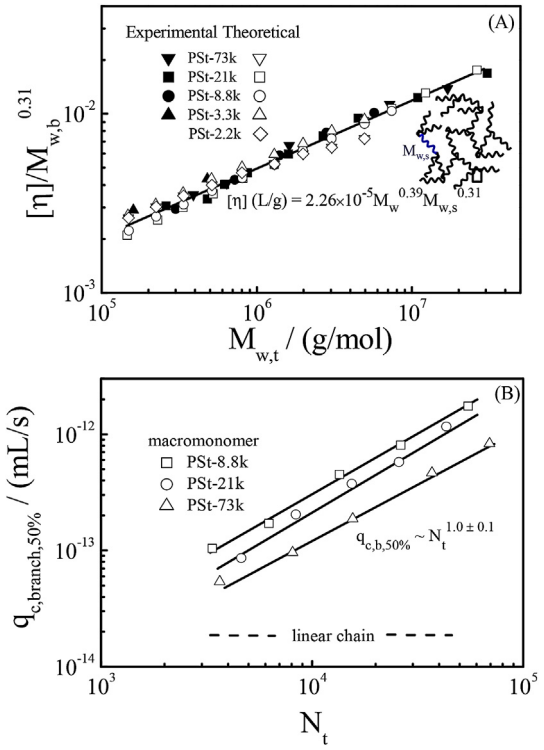

Fig. 9. (A) Overall weight-average molar mass (M_w) dependence of intrinsic viscosity ([η]) and (B) Overall polymerization degree (N_t) dependence of critical volumetric flow rate ($q_{c,branch,50\%}$) of hyperbranched polystyrenes with different subchain lengths in toluene at T = 25 °C (reported by Wu et al. [18,52]). Reproduced with permission [18,50].

with these model hyperbranched samples, we made it possible to answer how these hyperbranched chains pass through a cylindrical pore.

Fig. 9B shows a summary of the dependence of measured $q_{c,branch,50\%}$ on N_b and N_t. Quantitatively, $q_{c,branch,50\%}$ was found to be scaled to both N_b and N_t as $q_{c,branch} \sim N_t^{\gamma} N_b^{\varphi}$ with $\gamma = 1.0 \pm 0.1$ and $\varphi = -0.4 \pm 0.1$, which are different from those predicted by neither our unified description (Eq. (21)) nor de Gennes' derivation (Eq. (15)). It is worth mentioning that the observed transition is not as sharp as the first-order "coil-to-stretch" transition of linear chains mentioned, which is because even for a given overall molar mass, different arrangements of a given number of uniform subchains can lead to different hyperbranched chain structures (configuration diversity) and endow them with different deformabilities and critical volumetric flow rates. Physically, for a given overall molar mass, a smaller α in Eq. (20) means a more compact and less deformable chain conformation so that a higher volumetric flow rate is required to drag the chain into the pore, resulting in a stronger molar mass-dependent critical volumetric flow rate. Therefore, the higher measured γ value actually means that the real α value should be smaller. Putting the measured $\gamma = 1.0$ into Eq. (20), we are able to estimate that $\alpha \sim 3/8$, which is reasonable because the chain segments inside each blob are squeezed together with a more uniform chain density so that α should be lower than that for a free hyperbranched chain in solution. It is worth noting that such a discrepancy might also be traced back to the assumption of the blob as a non-draining sphere.

Intuitively, it is not hard to imagine that for a given N_b, a larger N_t will result in a larger deformation of a hyperbranched chain perpendicular to the flow direction from its initial size to the pore size, and thus involves a higher critical volumetric flow rate; while for a given N_t, a smaller N_b will lead to a higher branching degree, and subsequently a weaker deformability and a higher critical volumetric flow rate.

Recently, Brochard-Wyart et al. [51] predicted a novel characterization method to measure the unknown molecular parameters of hyperbranched polymers by using the finite length channel. The basic idea is that randomly branched polymers exhibit a passing/clogging transition across the nanochannel as a function of the channel length (Fig. 10). This critical channel size depends on the degree of the branching, whereby allowing the extraction of the branching information of the molecule. This new method is attracting because only one stretchable nanochannel is enough to separate polymer chains with different branching densities, while how to prepare membrane with different channel sizes and lengths may be not an easy task. Nevertheless, the most exciting implications from both experimental and theoretical studies mentioned above are that ultrafiltration characterization may provide more information of molecular parameters of hyperbranched polymers, compared to the generally adopted nuclear magnetic resonance and gel permeation chromatography techniques.

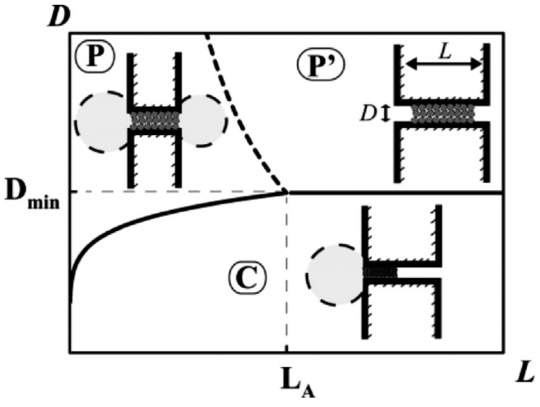

Fig. 10. Diagram of the passing–clogging transition of randomly branched chains (reported by Brochard-Wyart et al. [51]). Reproduced with permission [51].

4.5. Translocation of a microgel: effect of the degrees of swelling and cross-linking

The scope of discussion of this perspective is limited to individual polymer chains with different chain topologies, but one can still regard a microgel as an intramolecular cross-linked single chain with an infinite molar mass. To our knowledge, the experimental investigation of microgel translocation through cylindrical pores under biologically relevant pressure differentials was first reported by Lyon et al. [55], where two well-defined microgels made of N-isopropylacrylamide (NIPAM) and acrylic acid (AA, 10 mol%) with a similar size but different pH-dependent compressibilities were prepared to investigate the generality of the translocation phenomenon (Fig. 11). Interestingly, it was observed that the microgels under swollen state (pH = 7) could easily pass through nanopores with their pore size tenfold smaller than the unperturbed microgel diameter; in contrast, the de-swollen microgels (pH = 3) are almost retained by nanopores due to the rigid structure and limited compressibility (Fig. 11 B). Furthermore, they pointed out that increasing the microgel cross-linker content to 3% mol did not notably inhibit translocation.

It is worth noting that the study on the translocation of microgels through nanopores has received increasing attention in recent years [55–62], which is understood because the softness of nanoparticles is relevant in processes such as phagocytosis, endocytosis, kidney filtration and drug delivery [63,64]. Actually, the

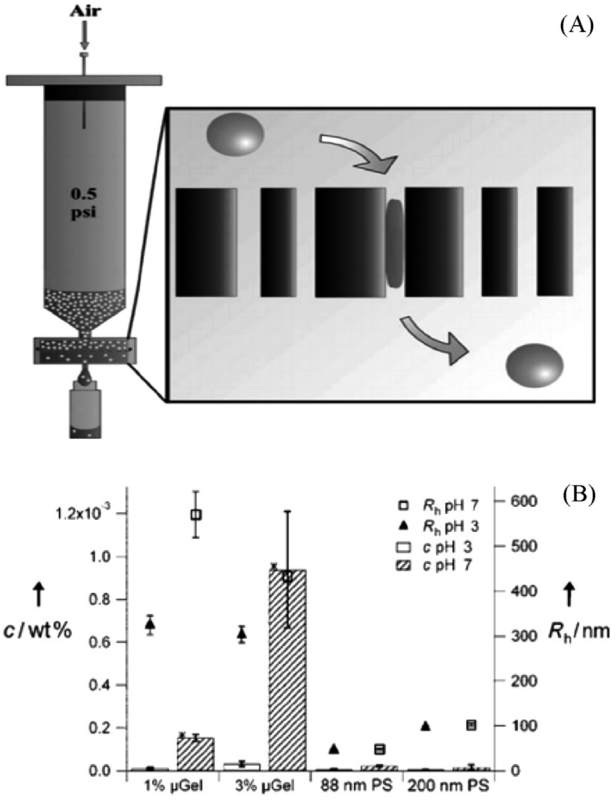

Fig. 11. (A) Schematic illustration of filtration setup and microgel filtration through a track-etch membrane; and (B) Filtration comparison of microgels with degrees of cross-linking of 1% and 3% mol, 88 nm polystyrene, and 200 nm polystyrene particles (0.01 wt %) (reported by Lyon et al. [55]). Reproduced with permission [55].

deformability of microgel is dominated by the properties of the microgel, such as internal density of charged groups, chain flexibility, and strength of the solvent–polymer interactions. These properties can be tuned to adjust microgel mechanics in order to control response to the surrounding (mechanical) environment for biologically relevant applications.

However, one problem that cannot be ignored is that the co-monomers and cross-linkers polymerized in the microgel particles by the common precipitation polymerization usually do not have a uniform distribution within the particles, which in turn have a profound effect on the microgel properties such as the mesh size distribution, swelling, stability, optical and mechanical properties [65–69]. The heterogeneous characteristic of prepared microgels also makes the study of translocation of microgels through nanopores less reliable and reproducible, compared with those of polymer chains with well-defined structures. In other words, the preparation of homogenously cross-linked microgels is the priority before any possible structure-property study.

5. Applications of ultrafiltration technique in related research fields

5.1. Separation of polymer chains with different topologies in a mixed solution

By understanding the ultrafiltration behavior of an individual polymer chain with a specific configuration in depth, one may really realize the purification and separation of polymer chains within a polymer mixture based on different structural parameters by ultrafiltration technique in our practical research work. Our group made much effort in this aspect [18,25]. The first straightforward example is the separation of a mixture of linear and star chains [25]. As shown in Fig. 12A and B, the linear chains could pass through nanopores at a lower volumetric flow rate no matter whether they are smaller (Fig. 12A, Star-41) or larger (Fig. 12B, Star-3) than the star chains. This is because our previous results clear demonstrated that $q_{c,linear}$ is independent of the chain length for a linear chain while $q_{c,star}$ increases with the arm number for a star chain. Furthermore, the separation of a mixed solution containing two kinds of hyperbranched chains with a similar hydrodynamic size but different branching densities, where the branching density of HB-3.3k chain is 21 times larger than that of HB-73k chain was also successfully achieved [18]. The results (Fig. 12C) clearly demonstrated that HB-73k chains could firstly pass through the nanopores due to their lower degree of branching. These two separation experiments verify the practicability of such an ultrafiltration method in the separation and fractionation of a mixture of polymer chains with different topologies and branching densities.

5.2. Rapid transformation of polymer chain aggregated structures

The discussion in previous sections on translocation has mainly focused on individual polymer chains with different topologies. Nevertheless, the translocation of the aggregated or self-assembled polymer chains with a larger dimensional scale has been reported in literature with only few examples so far [70–72]. It is worth noting that the investigation on how polymer aggregated structure passes through a nanopore is not only challenging in the field of ultrafiltration, but also may offer a strategy to tailor the morphology of polymer aggregates.

The first attempt was made by our group to study how the ultrafiltration process affects the morphology of polymeric micelles as it is still unknown whether the shear force can induce the rupture or transformation of polymeric aggregates if their sizes are larger than the pore size [73]. Diblock copolymer polystyrene-*b*-polyisoprene (PS-*b*-PI) could self-assemble into spherical micelles in *n*-hexane (a poor solvent for the PS block, but good solvent for PI block) with hydrodynamic radius larger than the nanopore. It was found that the ultrafiltration of polymeric micelles made of PS_{180}-*b*-PI_{500} through smaller nanopores is possible as long as the hydrodynamic force applied to each arm is sufficiently strong to overcome the interaction among the insoluble PS blocks in the core (Fig. 13A) [73]. The results clearly demonstrated that both the lengths of the soluble and insoluble blocks strongly affect the interaction among insoluble PS blocks. Moreover, the interaction strength could be quantitatively estimated by converting the volumetric flow rate-dependent retention distribution into the distribution of hydrodynamic force $[f(f_h)]$ as $f_h \sim \eta L_e q/D^2$ (Fig. 13B).

Our further study demonstrated that the ultrafiltration of block copolymer solution in its spherical micelles phase can also induce a morphological transformation of polymeric aggregates, i.e., a sphere-to-cylinder transition to form long worm-like micelles [70]. Fig. 14 shows a number of cylindrical micelles were observed after extrusion of PS_{170}-b-PI_{140} diblock copolymer solution in *n*-hexane/THF with 2.8 vol% THF content through 20 nm nanopores. By delicately tuning of the block copolymer composition, chain length and solvent quality of the micelles solution, the degree of softness of spherical micelles could be carefully controlled. As extrusion started, such soft spheres were squeezed into the nanopore and underwent an inter-micelle fusion inside the nanopore while more

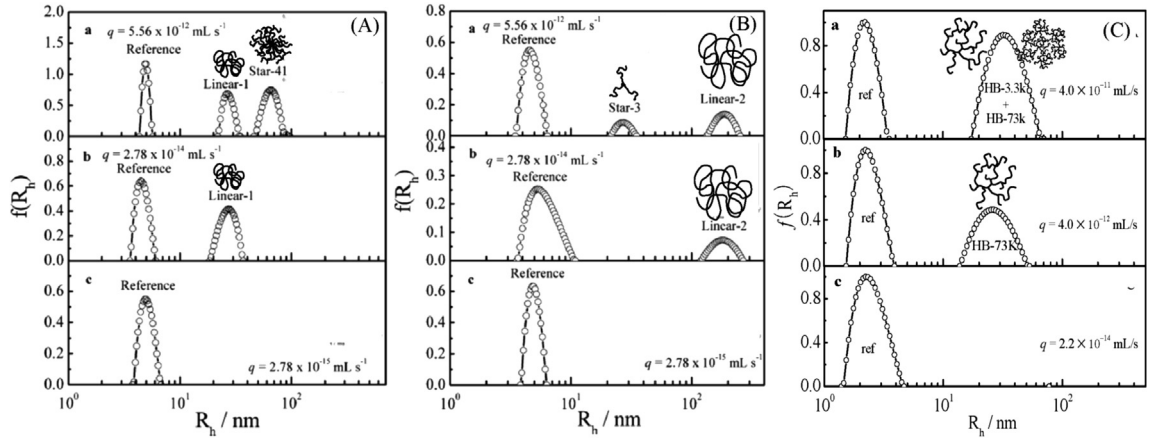

Fig. 12. Hydrodynamic radius distribution of a mixture of (A) reference, linear, and star-41 chains, (B) reference, linear-2, and star-3 chains, and (C) linear reference and two hyperbranched chains (HB-3.3k, and HB-73k) in toluene after the solution is extruded through nanopores under different volumetric flow rates (reported by Wu et al. [18,25]). Reproduced with permission [18,25].

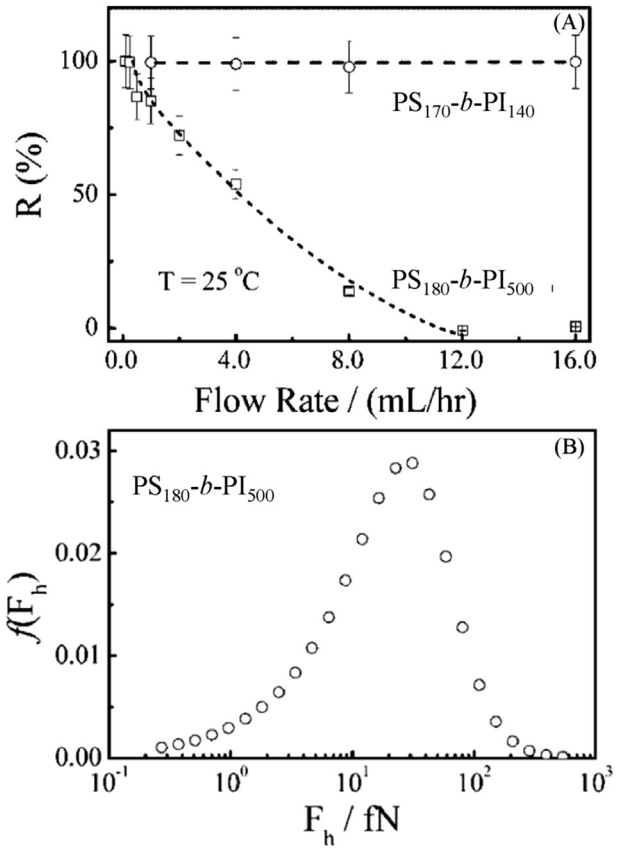

Fig. 13. (A) Macroscopic flow rate dependence of relative retention concentration $[(C_0 - C)/C_0$, i.e., $R(\%)]$ of polymeric micelles made of diblock PS_{170}-*b*-PI_{140} and PS_{180}-*b*-PI_{500}; and (B) Distribution of hydrodynamic force ($f(F_h)$) required to rupture polymeric micelles made of diblock PS_{180}-*b*-PI_{500} in *n*-hexane at $T = 25.0$ °C (reported by Wu et al. [73]). Reproduced with permission [73].

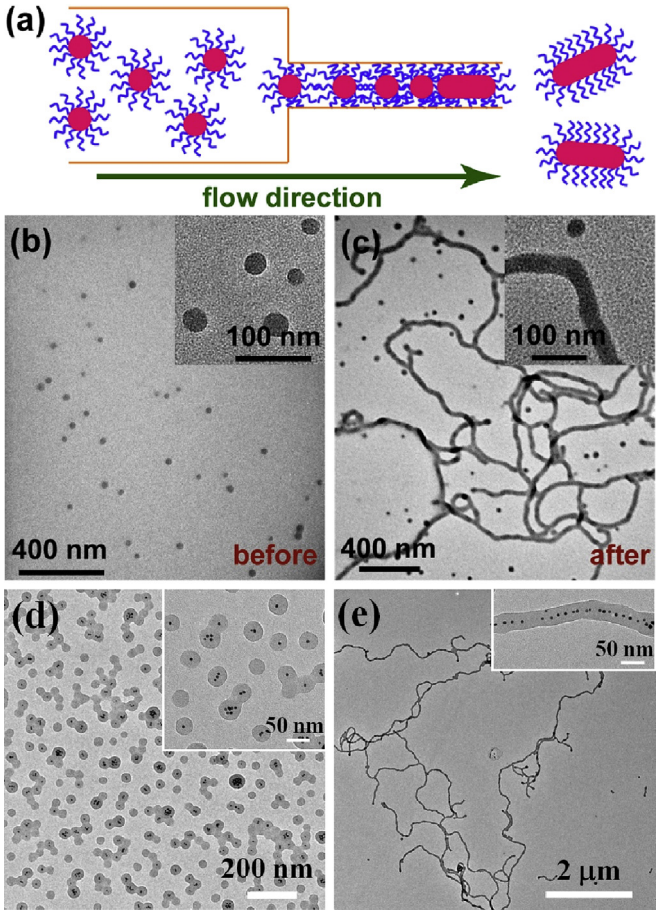

Fig. 14. (a) Schematic showing the extrusion process; (b and c) TEM images of the micelles before and after the extrusion through 20 nm nanopores; and (d and e) TEM images of the gold nanoparticles hybrid spherical micelles before and after the extrusion through 20 nm nanopores (reported by Wu et al. [70,72]). Reproduced with permission [70,72].

spherical micelles were accumulated at the pore entrance, resulting in a rearrangement of individual micelles into long cylindrical micelles (Fig. 14C). Base on the same scheme, we eventually produced long cylindrical hybrid nanofibers loaded with small gold nanoparticles, as shown in Fig. 14E [72]. This simple preparation method can be further modified to produce more functional polymeric "nanowires".

Recently, Qiu and his coworkers investigated the behavior of one-dimensional poly(3-alkylthiophenes) (P3ATs)-based nanofibers during ultrafiltration [71]. It was found that both the concentration and flow field have crucial influences on the morphology after ultrafiltration (Fig. 15A). Namely, a fiber-to-cluster transition was observed when the nanofibers in solution with the concentration above a critical value passed through the nanopores under a strong flow field (Fig. 15B). While under a weak flow field or the solution concentration below the critical concentration, the nanofibers maintained the one-dimensional morphology after ultrafiltration (Fig. 15C). The Zimm time (t_z) and the passing time (t_p) of the nanofibers were compared to explain the way the nanofibers pass through the nanopores under different flow fields. Compared to our observed sphere-to-cylinder transition, this work clearly demonstrates the possibility of utilizing ultrafiltration method to realize the inverse cylinder-to-sphere transition, which greatly enriches the strategy of tailoring the morphology of polymer aggregates.

6. Summary and outlook

Although the translocation behavior of polymer linear chains through a cylindrical pore has been theoretically discussed since the 1960s, only since the 1980s, significant experimental progress in the understanding of the ultrafiltration behavior of polymer chains with different topologies has been achieved due to the development of polymer synthetic technology and the improvement of membrane manufacturing technology. The achieved results clearly demonstrate whether a polymer chain can pass through a nanopore with its size smaller than the chain size is mainly dependent on the structures of the polymer chain and the nanopore, instead of the chain size. In addition, the interaction among flow fields of different pore entrances may greatly affect the sharpness of the transition process during translocation, namely, common single-layer membranes generally result in a smooth transition, while a sharp transition is expected when special double-layer membranes are adopted.

Generally speaking, both the polymer chain with a lower branching density and the pore with a larger size will lead to a weaker confinement and a corresponding lower critical volumetric flow rate (q_c). More specifically, the critical volumetric flow rate is dominated by the specific blob size of each confined chain inside the nanotube, which can be extracted from the counterbalance of confinement and hydrodynamic forces ($f_c = k_BT/\xi$ and $f_h = 3\pi\eta u l_e$) on individual "blobs". The experimental results demonstrate, for linear chain, $q_{c,linear}$ is chain length independent; for star chain, $q_{c,star}$ increases with the arm number, but irrelevant with the arm length; while for hyperbranched chain, $q_{c,hyperbranched}$ increases with the overall degree of polymerization of the entire chain, but decreases

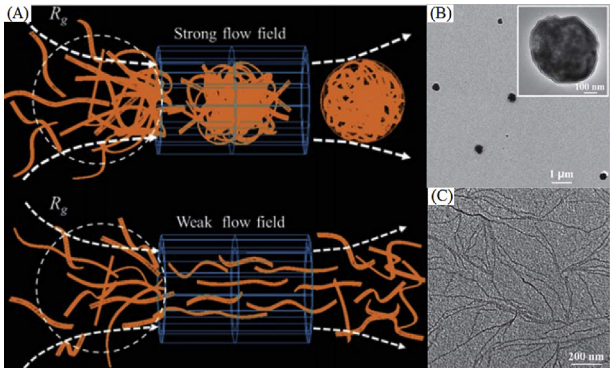

Fig. 15. (A) Schematic representation of nanofibers passing through a nanopore under a strong and a weak flow field; (B) TEM image of the clusters formed in the initial 0.2 g/L poly(3-butylthiophene)-b-poly(3-dodecylthiophene) (P3BT-b-P3DDT) solution after ultrafiltration at a volumetric flow rate of 0.25 mL/s; and (C) TEM image of the nanofibers formed in the initial 0.2 g/L P3BT-b-P3DDT solution after ultrafiltration at a volumetric flow rate of 0.01 mL/s (reported by Qiu et al. [71]). Reproduced with permission [71].

with the degree of polymerization of the branching subchain; for microgel, $q_{c,microgel}$ increases with the degree of swelling but slightly depends on the degree of cross-linking. These experimental findings establish a solid foundation for further applying the ultrafiltration method into some practical processes, such as the separation of polymer chain mixture and the rapid transformation among various polymer chain aggregated structures.

After understanding how linear, star and hyperbranched chains as well as well-defined microgel structure pass through a nanopore in depth, the investigation emphasis in future should focus on the other two kinds of model polymers, i.e., comb-like and dendrimer-like polymers. So far, it is still unclear that 1) for a comb-like chain, how the chain lengths of the backbone and the grafting subchain, and the chain length between two neighboring branching points affect its ultrafiltration behavior; 2) for a dendrimer-like chain, how the generation number (G) and the chain length of each generation affect its ultrafiltration behavior. However, how to prepare model samples with controlled parameters will be a real challenge in polymer synthesis.

Considering the achieved results have already indicated the possibility of applying the ultrafiltration technique into the separation of polymer chain mixtures and the rapid transformation of different polymer aggregated structures, more attention should be paid on the development of commercially available ultrafiltration experimental apparatus; while the preparation of ultrafiltration membrane with uniform pore size, controlled length, large flux and high strength will be another challenge.

Acknowledgment

The authors thank Prof. Weidong He, Prof. Liangzhi Hong, Dr Hui Ge and other colleagues for their support and contribution to the related work described here. For financial support, the Ministry of Science and Technology of China Key Project (2012CB933802), the National Natural Scientific Foundation of China Projects (20934005 and 51173177), and the Hong Kong Special Administration Region Earmarked Projects (CUHK4036/11P, 2130281/2060431; CUHK4035/12P, 2130306/4053005; and CUHK7/CRF/12G, 2390062) is gratefully acknowledged.

References

[1] Vilgis T, Haronska P, Benhamou M. J Phys II Fr 1994;4:2187–96.
[2] Casassa EF, Tagami Y. Macromolecules 1969;2:14–26.
[3] de Gennes PG. J Chem Phys 1974;60:5030–42.
[4] Pincus P. Macromolecules 1976;9:386–8.
[5] Daoudi S, Brochard F. Macromolecules 1978;11:751–8.
[6] Gay C, de Gennes PG, Raphael E, Brochard-Wyart F. Macromolecules 1996;29:8379–82.
[7] de Gennes PG. Adv Polym Sci 1999;38:92–106.
[8] Peterlin A. Pure Appl Chem 1966;12:563–86.
[9] Wang G, Chen HW, Oktay Y, Zhang J, Allen EL, Smith GM, et al. Cell 2010;142:456–67.
[10] Wu C. Macromolecules 2012;45:4422–4.
[11] Talaga DS, Li J. J Am Chem Soc 2009;131:9287–97.
[12] Pomposo JA, Perez-Baena I, Buruaga L, Alegría A, Moreno AJ, Colmenero J. Macromolecules 2011;44:8644–9.
[13] Teraoka I. Macromolecules 2004;37:6632–9.
[14] Wang Y, Teraoka I, Hansen FY, Peters GnH, Hassager O. Macromolecules 2010;44:403–12.
[15] Yong H, Zhang H, Xie Y, Yang H. Soft Matter 2013;9:3565–77.
[16] Wu C, Li LW. Polymer 2013;54:1463–5.
[17] Yong H, Wang Y, Yuan S, Xu B, Luo K. Soft Matter 2012;8:2769–74.
[18] Li L, He C, He W, Wu C. Macromolecules 2012;45:7583–9.
[19] Ledesma-Aguilar R, Sakaue T, Yeomans JM. Soft Matter 2012;8:4306–9.
[20] Ledesma-Aguilar R, Sakaue T, Yeomans JM. Soft Matter 2012;8:1884–92.
[21] Ge H, Pispas S, Wu C. Polym Chem 2011;2:1071–6.
[22] Freed KF, Wu C. Macromolecules 2011;144:9863–6.
[23] Freed KF. J Chem Phys 2011;135:144902.
[24] Beguin L, Grassl B, Brochard-Wyart F, Rakib M, Duval H. Soft Matter 2011;7:96–103.
[25] Ge H, Wu C. Macromolecules 2010;43:8711–3.
[26] Ge H, Jin F, Li J, Wu C. Macromolecules 2009;42:4400–2.
[27] Kolomeisky AB. Biophys J 2008;94:1547–8.
[28] Jin F, Wu C. Phys Rev Lett 2006;96:237801.
[29] Sakaue T, Raphaël E, Gennes PGd, Brochard-Wyart F. Eur Phys Lett 2005;72:83–8.
[30] Gay C, Raphael E. Adv Colloid Interface Sci 2001;94:229–36.
[31] Beerlage MAM, Heijnen ML, Mulder MHV, Smolders CA, Strathmann H. J Membr Sci 1996;113:259–73.
[32] Adamski RP, Anderson JL. J Polym Sci Polym Phys 1987;25:765–75.
[33] Anderson JL. J Polym Sci Polym Phys 1985;23:191–7.
[34] Long TD, Anderson JL. J Polym Sci Polym Phys 1984;22:1261–81.
[35] Nguyen QT, Neel J. J Membr Sci 1983;14:111–27.
[36] Muthukumar M. Phys Rev Lett 2001;86:3188–91.
[37] Wong CTA, Muthukumar M. Biophys J 2008;95:3619–27.
[38] Wong CTA, Muthukumar M. J Chem Phys 2008;128:154903.
[39] Fox ME, Szoka FC, Fréchet JMJ. Acc Chem Res 2009;42:1141–51.
[40] Janeshitz-Kriegl HJ. Adv Polym Sci 1969;6:170–86.
[41] Zimm BH. J Chem Phys 1956;24:269–78.
[42] Teraoka I. Polymer solution. New York: John Wiley & Sons, Inc; 2002.
[43] de Gennes PG. Biopolymers 1968;6:715–29.
[44] Zimm BH, Stockmayer WH. J Chem Phys 1949;17:1301–14.
[45] Isaacson J, Lubensky TC. J Phys Lett 1980;41:469–71.
[46] Brochard-Wyart F, de Gennes PG. C R Acad Sci Paris 1996;323II:473–9.
[47] Dondos A, Papanagopoulos D, de Gennes PG, Brochard-Wyart F. Macromol Theory Simul 1999;8:147–50.
[48] Ripoll M, Winkler RG, Gompper G. Phys Rev Lett 2006;96:188302.
[49] Meunier DM, Stokich TM, Gillespie D, Smith PB. Macromol Symp 2007;257:56–70.
[50] Li L, Lu Y, An L, Wu C. J Chem Phys 2013;138:114908.
[51] Sakaue T, Brochard-Wyart F. ACS Macro Lett 2014;3:194–7.
[52] Nikoubashman A, Likos CN. J Chem Phys 2010;133:074901.
[53] Render S. J Phys A: Math Gen 1979;12:L239.
[54] Lu Y, An L, Wang ZG. Macromolecules 2013;46:5731–40.
[55] Hendrickson GR, Lyon LA. Angew Chem Int Ed 2010;49:2193–7.
[56] Holden DA, Hendrickson GR, Lan WJ, Lyon LA, White HS. Soft Matter 2011;7:8035–40.
[57] Kersey FR, Merkel TJ, Perry JL, Napier ME, DeSimone JM. Langmuir 2012;28:8773–81.
[58] Pevarnik M, Schiel M, Yoshimatsu K, Vlassiouk IV, Kwon JS, Shea KJ, et al. ACS Nano 2013;7:3720–8.
[59] Saxena S, Hansen CE, Lyon LA. Acc Chem Res 2014;47:2426–34.
[60] Holden DA, Hendrickson G, Lyon LA, White HS. J Phys Chem C 2011;115:2999–3004.
[61] Lan WJ, Holden DA, White HS. J Am Chem Soc 2011;133:13300–3.
[62] Lan WJ, Holden DA, Zhang B, White HS. Anal Chem 2011;83:3840–7.
[63] Beningo KA, Wang YI. J Cell Sci 2002;115:849–56.
[64] Banquy X, Suarez F, Argaw A, Rabanel JM, Grutter P, Bouchard JF, et al. Soft Matter 2009;5:3984–91.
[65] Kratz K, Hellweg T, Eimer W. Polymer 2001;42:6631–9.
[66] Kratz K, Lapp A, Eimer W, Hellweg T. Colloid. Surf A 2002;197:55–67.
[67] Saunders BR. Langmuir 2004;20:3925–32.
[68] Stieger M. J Chem Phys 2004;120:6197.
[69] Acciaro R, Gilanyi T, Varga I. Langmuir 2011;27:7917–25.
[70] Chen Q, Zhao H, Ming T, Wang J, Wu C. J Am Chem Soc 2009;131:16650–1.
[71] Pan Z, Ge J, Li W, Peng J, Qiu F. Soft Matter 2012;8:9981–4.
[72] Chen Q, Wang J, Shao L. Macromol Rapid Comm 2013;34:1850–5.
[73] Hong L, Jin F, Li J, Lu Y, Wu C. Macromolecules 2008;41:8220–4.

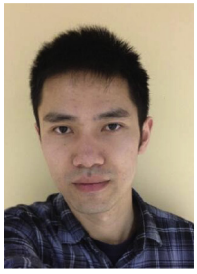

Lianwei Li obtained his PhD in 2014 under the supervision of Professor Chi Wu at The University of Science and Technology of China. Currently he is a postdoctoral research associate with Prof. Luping Yu at The University of Chicago.

Qianjin Chen obtained his PhD in 2013 under the supervision of Professor Chi Wu at The Chinese University of Hong Kong. Currently he is a postdoctoral research associate with Prof. Henry S. White at The University of Utah.

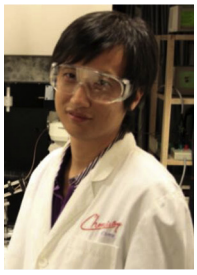

Fan Jin obtained his PhD in 2007 followed by one and half years postdoctoral experience under the supervision of Professor Chi Wu at The Chinese University of Hong Kong. He spent additional three years for his postdoctoral research in United States (University of Illinois and University of California) under the supervision of Professor Gerard Wong. In 2011, he joined the Hefei National Laboratory for Physical Sciences at the Microscale in University of Science and Technology of China as an independent investigator.

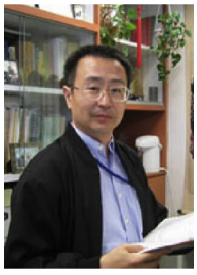

Chi Wu obtained his PhD in 1987 followed by two-year postdoctoral experience under the supervision of Professor Benjamin Chu at the State University of New York at Stony Brook. He moved to BASF (Ludwigshafen, Germany) in 1989; first as an Alexander von Humboldt Fellow for one year with Dr. Dieter Horn and then as the supervisor of laser light-scattering laboratory. In 1992, he joined the Department of Chemistry at the Chinese University of Hong Kong as a Lecturer and was promoted to be a Chair Professor of Chemistry and Honorary Professor of Physics in 1999. Recently, he has been appointed as a Wei Lun Chair Professor of Chemistry since 2010.